Progress In Electromagnetics Research C, Vol. 67, 31–40, 2016

An Independently Tunable Dual-Band Bandpass Filter Using a Center Shorting-Stub-Loaded Resonator

Fei Liang*, Weiwei Cai, Wenzhong Lu, Li Deng, and Xiaofei Zhai

Abstract—This paper presents an independently tunable dual-band bandpass filter based on center shorting-stub-loaded resonators. The center shorting-stub-loaded resonator is a dual-mode resonator that generates odd-even modes approximately equal and coupled when the shorting stub is very short. Two different sizes of center shorting-stub-loaded resonators produce two separated resonant frequencies, which are mutually independent. The coupling between the source and load is introduced in the circuit by designing an appropriate coupling structure, and the skirt selectivity of the filter is greatly improved. Four varactor diodes are placed at the two open-circuit ends of the center shorting-stub-loaded resonator to control the two separated resonant frequencies. A prototype of a tunable dual-band filter with Chebyshev response is designed and fabricated. The measured results are in good agreement with the full-wave simulated results. Results show that the first passband varies in a frequency range from 0.81 GHz to 0.95 GHz with a 3 dB fractional bandwidth of 4.2% to 5%, whereas the second passband can be tuned from 1.51 GHz to 1.79 GHz with a 3 dB fractional bandwidth of 6.8% to 8%.

1. INTRODUCTION

Multiband microwave components are important as fundamental parts in multiband wireless communication systems. Particularly, multiband bandpass filters (BPFs) with tunable center frequency have attracted more and more attention because of their potential to meet the present requirements of system size and complexity.

Recently, a few methods have been applied in design of microstrip tunable filter. Such as yittrium-iron-grant (YIG) [1], radio-frequency microelectromechanical system (RF-MEMS) [2–5], ferroelectric devices [6, 7], p-i-n diodes [8], and semiconductor varactor diodes [9–12]. The semiconductor varactor diodes are widely used in the tunable microstrip filters because of their low cost, high tuning speed and reliability [13–15]. In [16], a tunable bandpass filter with controllable dual passbands was proposed. However, the two passbands are dependently tunable. Chaudhary et al. developed a tunable dual-band filter with a fixed first passband and controllable second passband. However, the filter has a large circuit size and relatively complicated bias circuit [17]. In [18], a dual-band tunable bandpass filter with independently controllable dual passbands based on asymmetric $\lambda/4$ resonator pairs was proposed. In this design, the coupling coefficients depended on the spaces between the two resonators. When the spaces between the two resonators changed, the whole circuit also changed together.

In this paper, center shorting-stub-loaded resonators are utilized to form a dual-band BPFs with independently tunable passband center frequencies. The coupling coefficients between even- and odd-modes can be adjusted by changing the position of the via hole on the shorting stub. Two separated passbands are independently generated by two center shorting-stub-loaded resonators with different electric lengths. Both the passbands center frequencies of the dual-band filter can be tuned

Received 31 May 2016, Accepted 26 August 2016, Scheduled 2 September 2016

* Corresponding author: Fei Liang (liangfei@mail.hust.edu.cn).

The authors are with the School of Optical and Electronic Information, Huazhong University of Science and Technology, Wuhan 430074, China.

independently by tuning varactor diodes placed at the two open-circuit ends of the resonator. The circuit structure of the proposed structure is relatively simple. A prototype tunable dual-band filter is designed, fabricated, and measured to provide an experimental validation on the proposed filters.

2. THEORY AND DESIGN EQUATIONS

2.1. Characteristics of the Proposed Resonator

Figure 1(a) shows the basic structure of the proposed resonator. The structure is symmetrical, thus, the even–odd mode analysis method can be used for theoretical analysis of the resonant frequencies.

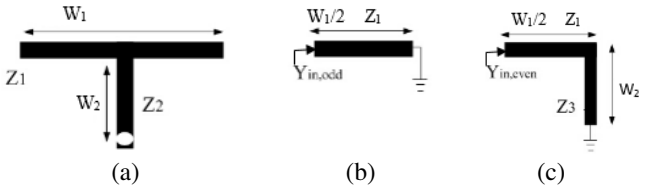

Figure 1. Structure of the proposed resonator. (a) Basic structure of the resonator. (b) Odd-mode excitation equivalent circuit. (c) Even-mode excitation equivalent circuit.

A voltage null point exists along the symmetry plane when odd-mode excitation is applied to the ends of the proposed resonator. The proposed resonator can be represented by the equivalent half circuit shown in Figure 1(b) under odd-mode excitation condition. The odd-mode input admittance is presented as follows:

$$Y_{in,odd}=\frac{1}{jZ_1\tan(\beta W_1/2)} \tag{1}$$

According to the odd-mode resonance condition, resonant frequency can be determined as follows:

$$f_{odd}=\frac{2n-1c}{2W_1\sqrt{\varepsilon}} \tag{2}$$

Equation (2) indicates that the odd-mode resonant frequency fully depends on the transmission line length W_1. Moreover, the odd-mode resonant frequencies are not affected by the shorting stub connected at the center of the transmission line.

For the even-mode excitation, no current flows through the center of the transmission line. Under the even-mode condition, the proposed resonator can be represented by the equivalent half circuit shown in Figure 1(c). The even-mode input admittance is presented as follows:

$$Y_{in,even}=\frac{Z_1-Z_3\tan(\beta W_1/2)\tan(\beta W_2)}{jZ_1[Z_1\tan(\beta W_1/2)+Z_3\tan(\beta W_2)]} \tag{3}$$

According to even-mode resonance condition, resonant frequency can be determined as follows:

$$\tan(\beta W_1/2)\tan(\beta W_2)=\frac{Z_1}{Z_3} \tag{4}$$

Equation (4) indicates that the even-mode resonant frequency depends on both the transmission line length W_1 and shorting stub length W_2 connected at the center of the transmission line.

When the length of the shorting stub W_2 is near zero, $\tan(\beta W_2)=0$. Then, the even-mode input admittance is presented as follows:

$$Y_{in,even}=\frac{Z_1-Z_3\tan(\beta W_1/2)\tan(\beta W_2)}{jZ_1[Z_1\tan(\beta W_1/2)+Z_3\tan(\beta W_2)]}\approx\frac{1}{jZ_1\tan(\beta W_1/2)} \tag{5}$$

According to Equation (5), odd–even modes are approximately equal and mutually coupled when the length of the shorting stub W_2 is near zero, which is shown in Figure 2. The structure of the resonator is shown in Figure 3.

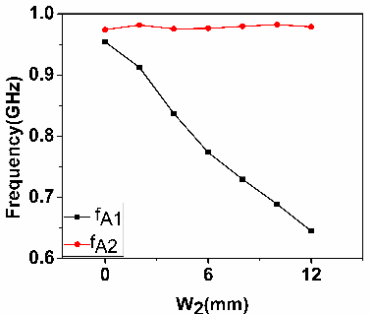

Figure 2. Resonant frequencies of odd–even modes.

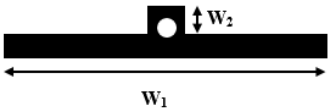

Figure 3. Structure of a single resonator.

2.2. Schematic of the shorting-stub-loaded tunable filter

In this section, the tunable dual-band filter schematic is shown in Figure 4. It consists of two shorting-stub-loaded resonators (A and B). The two shorting stubs are very short. Thus, each passband of the filter is formed by the coupling between odd and even modes. Both shorting-stub-loaded resonators can be seen as two-stage one-quarter wavelength resonators ($A1$ and $A2$, $B1$ and $B2$). The longer resonator, A, works at low frequency f_A; whereas the shorter resonator, B, works at high frequency f_B. The two resonators share the I/O feedlines, and these resonators are separated by the feedlines.

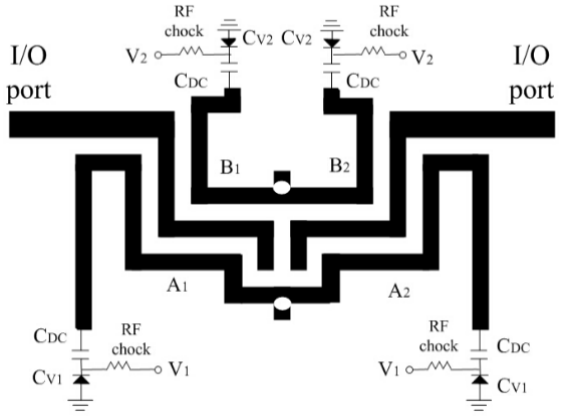

Figure 4. Schematic of the dual-band shorting-stub-loaded tunable filter.

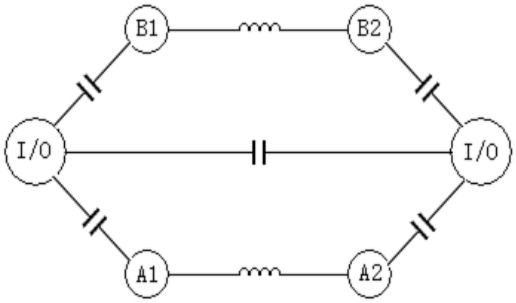

Figure 5. Equivalent topology of the designed filter.

The two open ends of the feedlines are close to each other to introduce the coupling between source and load, which is a capacitive coupling because the open ends have maximum electric field distribution. The positions of the via holes are changed to decrease the capacitive coupling, which makes the inductive coupling become the primary coupling. The equivalent topology, consisting of I/O ports, is shown in Figure 5. Nodes $A1$ and $A2$ denote the odd and even modes resonators of the first passband, whereas nodes $B1$ and $B2$ denote odd and even modes resonators of the second passband, respectively. The transmission zeros are introduced at both sides of each passband by the coupling between the source and load. The strength of the coupling between the source and load can be changed by adjusting the spacing between the two feedlines. Thus, the positions of transmission zeros can be controlled.

2.3. Characteristics of Center Shorting-stub-loaded Resonator Loaded by Varactor Diodes

Resonator A and resonator B have the same work principle, and resonator A is taken as an example. As shown in Figure 6, the two open ends of the resonator A are respectively welded with the varactor

diode C_{V1}, the DC block capacitor C_{DC} and the AC block inductance (RF chock). The resonator A is symmetrical, there is also a voltage null point exists along the symmetry plane, and it is shown in Figure 6(b). The resonant frequency can be determined as follows from the resonance condition:

$$Y_{in\_A1} = j\left[\omega C_{t1} Y_1 \cot\left(\frac{\beta_1 W_1}{2}\right)\right] \tag{6}$$

$$Y_{in\_A2} = j\left[\omega C_{t1} - Y_1 \cot\left(\beta_1 \frac{W_1+2W_2}{2}\right)\right] \tag{7}$$

where β is the propagation constant, and C_{t1} is the total capacitance of a series connection by DC block capacitor C_{DC} and varactor diode C_{V1}, which is given as follows:

$$C_{t1} = \frac{C_{V1} C_{DC}}{C_{V1} + C_{DC}} \tag{8}$$

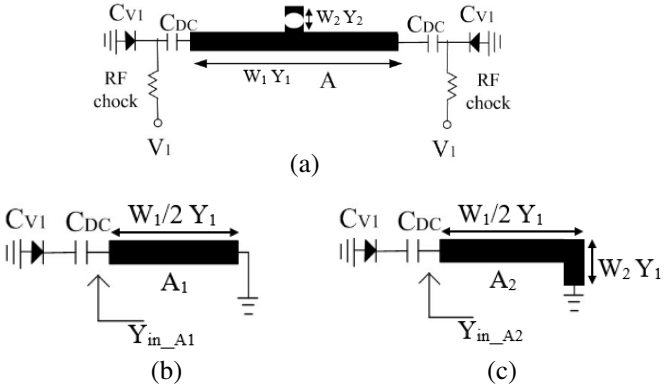

Figure 6. (a) Center shorting-stub-loaded resonator with varactor diodes. (b) Odd-mode equivalent circuit. (c) Even-mode equivalent circuit.

For the resonance condition, the resonant frequency can be determined as follows:

$$2\pi C_{t1} f_{A1} \tan\left(\frac{\pi f_{A1} W_1 \sqrt{\varepsilon}}{C}\right) = Y_1 \tag{9}$$

$$2\pi C_{t1} f_{A2} \tan\left[\frac{\pi f_{A2} \sqrt{\varepsilon}(W_1+2W_2)}{C}\right] = Y_1 \tag{10}$$

As seen from Equations (9) and (10), the odd-mode resonant frequency f_{A1} is determined by the transmission line length W_1 and the total capacitance Ct_1; the even-mode resonant frequency f_{A2} is

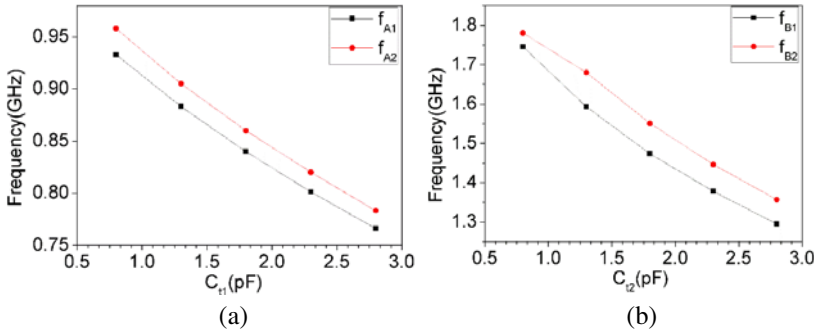

Figure 7. (a) Resonant frequency of resonator A varies with C_{t1}. (b) Resonant frequency of resonator B varies with C_{t2}.

determined by the transmission line length W_1, the shorting stub length W_2 and the total capacitance C_{t1}. When W_2 is near zero, the resonant frequencies (f_{A1} and f_{A2}) of odd-even modes are almost equal and mutually coupled and they can be tuned by varying C_{t1}. The same principle applies also to the resonator B. The relationship between the resonant frequency of the resonators (A and B) and the variable capacitance is shown in Figure 7. As seen from Figure 7, the resonant frequencies of the resonators (A and B) both decrease with the increasing of the variable capacitance.

2.4. External Quality Factors

The external quality factors can be discussed by half circuit because of the symmetric structure of the proposed filter. Figure 8 shows the basic configuration of the I/O coupling scheme.

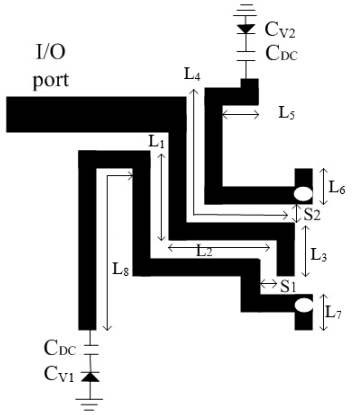

Figure 8. Circuit of I/O coupling scheme.

In this structure, feedline width, the distance between the feedline and the resonators, and coupling length have a great influence on the external quality factor. First, the electrical length of the microstrip and the value of the varactor diode are determined according to the working frequency. Then, the influence of the microstrip with various-size parameters (L_1, L_2, L_3, L_4 and S_1, S_2) on the external quality factor is investigated with HFSS software by referring to controlling variable method. We can simulate the high- and low-frequency I/O scheme because of the independence between these two parts caused by the feedlines. In this paper, we consider coupling spacing as a variable, and the other physical dimensions are fixed according to the following formula. Then, we can obtain the accurate values of the external quality factor $(Q_e)_A$ and $(Q_e)_B$, as shown in Figure 9.

$$(Q_e)_A = \omega_A/\Delta\omega_{A\pm 90^\circ} \tag{11}$$

$$(Q_e)_B = \omega_B/\Delta\omega_{B\pm 90^\circ} \tag{12}$$

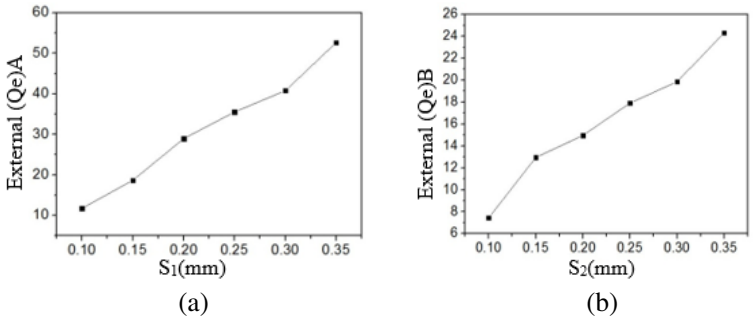

Figure 9. (a) Variation of $(Q_e)_A$ with S_1 and (b) variation of $(Q_e)_B$ with S_2 when $L_1 = 9\,\text{mm}$, $L_2 = 11.5\,\text{mm}$, $L_3 = 3\,\text{mm}$, $L_4 = 16.5\,\text{mm}$, $L_5 = 3.2\,\text{mm}$, $L_6 = 1.5\,\text{mm}$, $L_7 = 1.2\,\text{mm}$, $L_8 = 18.5\,\text{mm}$, $S_3 = 0.6\,\text{mm}$, $S_4 = 2.6\,\text{mm}$.

Q_e may increase when the spacing increases. We can easily obtain the changing tendency caused by coupling length by referring to the preceding method. When we calculate the required value of Q_e, we can synthetically analyze the preceding simulation results to achieve the Q_e value we need by choosing the appropriate physical dimensions of the spacing.

2.5. Coupling Coefficients (Ki)

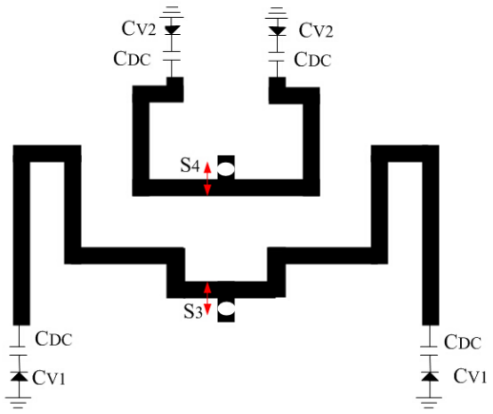

Figure 10. Coupling structure between two stages.

In the proposed filter, the shorting stub of the dual-mode resonator is very short. Thus, the shorting-stub-loaded resonator becomes equivalent to the two-pole quarter wavelength resonator. The position of the via hole can significantly affect the coupling coefficient. In this filter, we have two coupling schemes: one is for low frequency (K_A), whereas the other is for high frequency (K_B), as shown in Figure 10.

F_{A1} and f_{A2} are defined as the coupling separation modes for low frequency, whereas f_{B1} and f_{B2} are the coupling separation modes for high frequency. The coupling coefficient can be calculated with the following formula:

$$K_A = \frac{f_{A1}^2 - f_{A2}^2}{f_{A1}^2 + f_{A2}^2} \tag{13}$$

$$K_B = \frac{f_{B1}^2 - f_{B2}^2}{f_{B1}^2 + f_{B2}^2} \tag{14}$$

By HFSS software, the coupling coefficient variation with positions of via holes is shown in Figure 11, which indicates that the coupling coefficient increases when the via holes approach the ends of the shorting stubs.

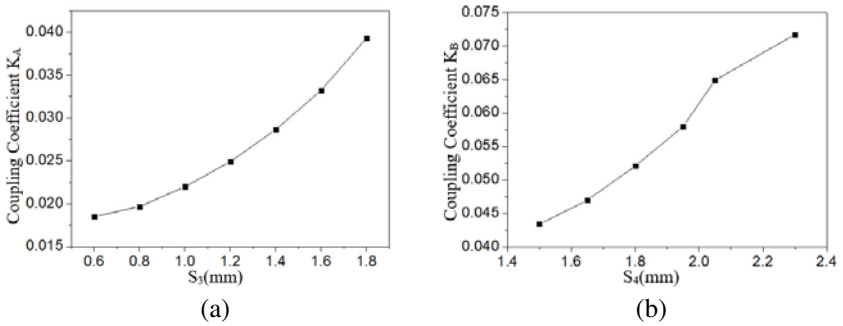

Figure 11. The influence of the positions of via-holes on coupling coefficient. (a) K_A and (b) K_B.

3. FILTER DESIGN AND MEASURED RESULT

To verify the aforementioned theory, a tunable dual-band filter with the following specifications was designed:

- First tuning passband: 0.8–0.95 GHz
- 3 dB fractional bandwidth (FBW) of the first passband: 4%–5%
- Second tuning passband: 1.55–1.75 GHz
- 3 dB FBW of the second passband: 7%–8%
- Insertion loss: less than 3.5 dB
- Number of poles: two
- Type: Chebyshev frequency response

The ultimate layout of the proposed filter is shown in Figure 4, and it is fabricated on the substrate, namely, Rogers 4350B, with a thickness of 0.762 mm, a dielectric constant of 3.5, and a loss tangent of 0.004. A complete fabricated filter is shown in Figure 12. This filter consists of two dual mode resonators and common input/output ports. Four capacitors functioning as DC blocking. A 500 nH inductance chip and a 10 Ω resistance are connected in a series in the DC bias circuit, which works as the reducing RF signal leakage networks. The four varactor diodes placed at the ends of resonators are SMV1405-079 of Skyworks Corporation. The capacitance of varactor diode varies from 2.67 to 0.63 pF when the value of the reverse bias voltage varies from 0 V to 30 V. However, it is not linear and the tunability of the proposed filter is not linear either. After repeated optimizations, the final physical parameters and component values of the filter are as follows: $L_1 = 9$ mm, $L_2 = 11.5$ mm, $L_3 = 3$ mm, $L_4 = 16.5$ mm, $L_5 = 3.2$ mm, $L_6 = 1.5$ mm, $L_7 = 1.2$ mm, $L_8 = 18.5$ mm, $S_1 = S_2 = 0.2$ mm, $S_3 = 0.6$ mm, $S_4 = 2.6$ mm, $C_{DC} = 56$ pF.

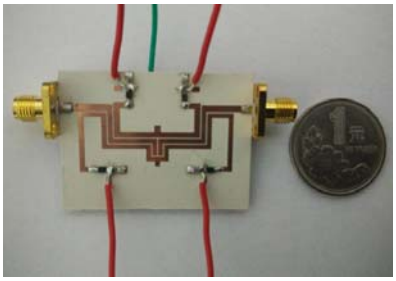

Figure 12. The photograph of the fabricated filter.

Figures 13(a) and (b) illustrate the simulation results of the S parameters when the value of C_{V1} is fixed as 1.1 pF and C_{V2} is set as 0.9, 1.25, and 1.7 pF. Figures 13(c) and (d) illustrate the simulation results of the S parameters when C_{V2} is fixed as 1.3 pF and C_{V1} is set as 0.7, 1.3, and 2.2 pF. As seen from Figure 13, the insertion losses of the two passbands are greater than −1 dB, and the return losses are less than −13 dB. The transmission zeros are introduced at both sides of the passbands. Thus, the stop band suppression is greatly improved. The position of the transmission zeros changes with the variation of the center frequency, and the good performance of the band rejection is always maintained. This phenomenon occurs because the transmission zeros are introduced by the special phase relationship between the main coupling and the coupling between source and load. When the values of varactor diodes vary, the phase shift around the resonant frequency remains unchanged. Thus, the transmission zeros move along with the resonant frequency.

The measurement is performed with Agilent Vector network analyzer E8362, and the results are illustrated in Figures 14 and 15. In Figure 14, the second passband frequency is fixed at 1.66 GHz with an insertion loss of −2.8 dB and a −3 dB FBW of 7.5% when the reverse bias voltage $V2$ is 17 V. In the meantime, the center frequency of first passband is tuned from 0.81 GHz to 0.95 GHz continuously as the variation of the reverse bias voltage $V1$ varies from 5 V to 28 V, and the insertion loss changes from

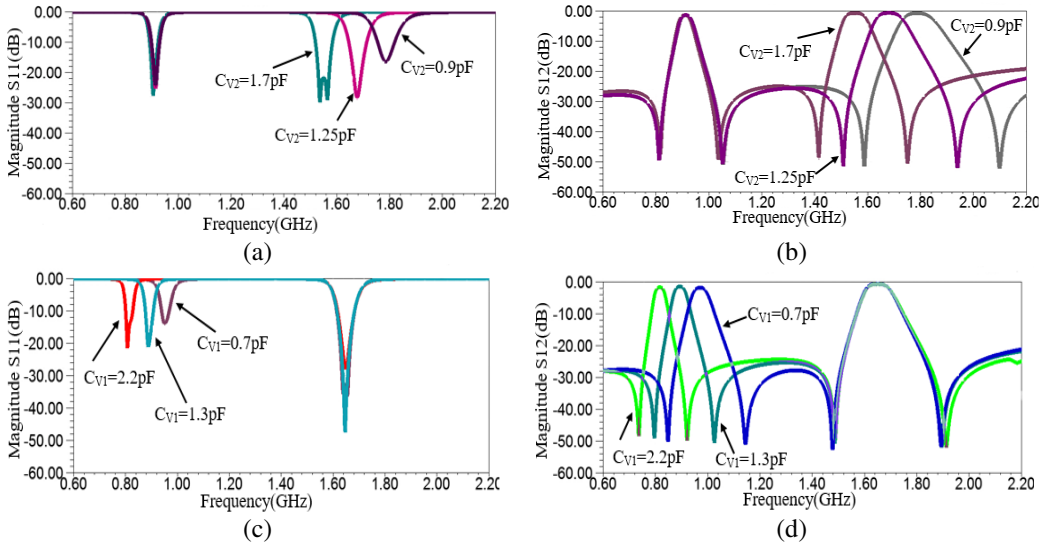

Figure 13. Simulation results of the tunable filter. (a) S_{11} and (b) S_{21} with tunable second passband; (c) S_{11} and (d) S_{21} with tunable first passband.

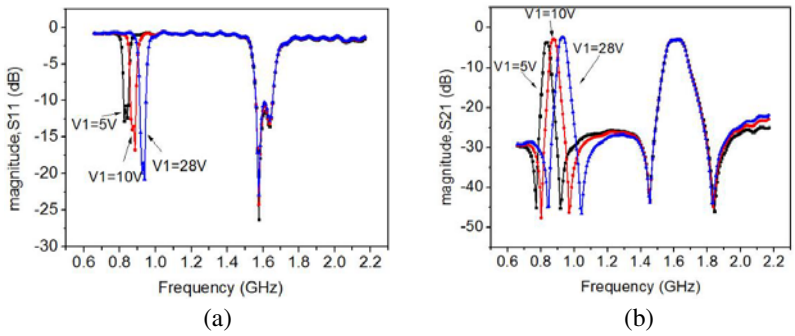

Figure 14. Measurement results of the tunable filter. (a) S_{11} and (b) S_{21} with tunable first passband.

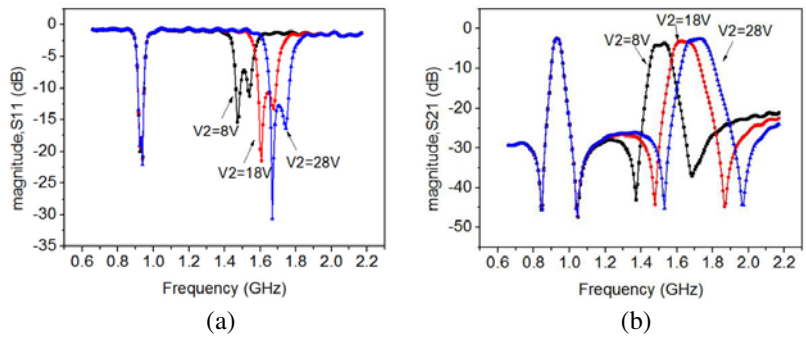

Figure 15. Measurement results of the tunable filter. (a) S_{11} and (b) S_{21} with tunable second passband.

−3.3 dB to −2.1 dB. The −3 dB FBW is maintained in the range of 4.2% to 5%. The return losses of the two passbands are both less than −13 dB in the tuning process.

As shown in Figure 15, the first passband frequency is fixed at 0.92 GHz with an insertion loss of −2.4 dB and a −3 dB FBW of 4.8% when the reverse bias voltage $V1$ is 25 V. In the meantime, the center frequency of the second passband is tuned from 1.51 GHz to 1.79 GHz continuously as the reverse bias voltage varies from 8 V to 28 V, and the insertion loss changes from −3.26 dB to −2.37 dB. The

−3 dB FBW is maintained in the range of 6.8% to 8%. The return losses of the two passbands are both less than −12 dB in the whole tuning process. Seen from the Figures 14 and 15, as the reverse bias voltages $V1$ and $V2$ gradually increase, the reflection coefficients S_{11} are becoming smaller, and the corresponding values of insertion loss S_{21} are also getting smaller. We think as the reverse bias voltages $V1$ and $V2$ gradually increase, the capacitance values of the varactor diodes are getting smaller, which may improve the degree of the impedance matching between the filter and external circuit and reduce the loss of reflection at the input ports.

In general, the measurement results keep consistent with the simulated results. However, the variation ranges of the two passbands are slightly different and the insertion loss is a little worse, which may result from the ignored parasitic parameters of the varactor diodes and the mechanical errors.

Table 1. Comparison for tunable dual-band filters.

	1st Passband		2nd Passband		Harmonic Suppression	Lumped Elements	
	Frequency (GHz)	Insertion Loss (dB)	Frequency (GHz)	Insertion Loss (dB)		Diodes	C_{DC}
[11]	1.5–1.8	3.02–4.8	2.45–2.80	2.78–4.6	Yes	6	6
[17]	0.85–1.2	1.32–3.4	1.40–2.14	1.80–3.80	Yes	6	4
[18]	0.88–1.12	1.65–4.3	1.51–1.81	3.11–3.9	No	4	4
This work	0.81–0.95	2.1–3.3	1.51–1.79	2.37–3.26	No	4	4

Table 1 shows the performance comparisons of the proposed tunable filter with other recently reported tunable filters in the literatures. According to Table 1, the main advantages of our proposed filter include the following: The coupling between source and load is introduced to generate transmission zeros and the skirt selectivity of the filter is greatly improved. The coupling coefficient can be easily adjusted by changing the position of the via hole on the shorting stub. The first and second pass-bands of our proposed filter are completely independently tuned with relatively simple tunable circuit.

4. CONCLUSION

In this paper, the tunable dual-band BPFs with independently tunable center frequency are demonstrated. The proposed structure is validated by both theoretical analysis and experiments. The experiment results are in good agreement with the theoretical predictions. The experimental results show that the first passband can be tuned from 0.81 GHz to 0.95 GHz with the 3 dB FBW maintained in the range of 4.2% to 5%. The second passband can be also tuned from 1.51 GHz to 1.79 GHz with the 3 dB FBW maintained in the range of 6.8% to 8%. The transmission zeros are introduced at both sides of each passband by the coupling between the source and load. In the tuning progress, the transmission zeros beside the both two passbands move with the variation of center frequencies, the skirt selectivity of the tunable dual-band passband filter is significantly improved.

REFERENCES

1. Wong, P. W. and I. C. Hunter, "Electronically reconfigurable microwave bandpass filter," *IEEE Transactions on Microwave Theory and Techniques*, Vol. 57, 3,070–3,079, 2009.
2. Entesari, K. and G. M. Rebeiz, "A differential 4-bit 6.5-10-GHz RF MEMS tunable filter," *IEEE Transactions on Microwave Theory and Techniques*, Vol. 53, 1,103–1,110, 2005.
3. Entesari, K. and G. M. Rebeiz, "A 12–18-GHz three-pole RF MEMS tunable filter," *IEEE Transactions on Microwave Theory and Techniques*, Vol. 53, No. 8, 2,566–2,571, 2005.
4. Huang, F., S. Fouladi, and R. R. Mansour, "High-tunable dielectric resonator filters using MEMS technology," *IEEE Transactions on Microwave Theory and Techniques*, Vol. 59, No. 12, 3,401–3,409, 2011.

5. Park, S. J., M. A. El-Tanani, I. Reines, and G. M. Rebeiz, "Low-loss 4–6-GHz tunable filter with 3-bit high-orthogonal bias RF-MEMS capacitance network," *IEEE Transactions on Microwave Theory and Techniques*, Vol. 56, No. 10, 2,348–2,355, 2008.
6. Nath, J., D. Ghosh, J. P. Maria, A. I. Kingon, W. Fathelbab, P. D. Franzon, and M. B. Steer, "An electronically tunable microstrip bandpass filter using thin-film Barium-Strontium-Titanate (BST) varactors," *IEEE Transactions on Microwave Theory and Techniques*, Vol. 53, No. 9, 2,707–2,712, 2005.
7. Jiang, H., B. Lacroix, K. Choi, Y. Wang, A. T. Hunt, and J. Papapolymerou, "*Ka* and *U* band tunable bandpass filters using ferroelectric capacitors," *IEEE Transactions on Microwave Theory and Techniques*, Vol. 59, No. 12, 3,068–3,075, 2011.
8. Liu, B., F. Wei, and X. Shi, "Reconfigurable bandpass filter based on net-type stepped-impedance resonator," *Electronics Letters*, Vol. 46, No. 22, 1,506–1,507, 2010.
9. Chen, J.-X., J. Shi, Z.-H. Bao, and Q. Xue, "Tunable and switchable bandpass filters using slot-line resonators," *Progress In Electromagnetics Research*, Vol. 111, 25–41, 2011.
10. Wang, Y.-Y., F. Wei, H. Xu, and X. W. Shi, "A tunable 1.4-2.5 GHz bandpass filter based on single mode," *Progress In Electromagnetics Research*, Vol. 135, 261–269, 2013.
11. Chaudhary, G., Y. Jeong, and J. Lim, "Dual-band bandpass filter with independently tunable center frequencies and bandwidths," *IEEE Transactions on Microwave Theory and Techniques*, Vol. 61, No. 1, 107–116, 2013.
12. Kim, G. R., "A novel compact tunable bandpass filter loaded varactor diode on the DGS," *Journal of Information and Communication Convergence Engineering*, Vol. 8, No. 3, 263–266, 2010.
13. Feng, T., Y. Li, H. Jiang, W. Li, F. Yang, X. Dong, and H. Chen, "Tunable single-negative metamaterials based on microstrip transmission line with varactor diodes loading," *Progress In Electromagnetics Research*, Vol. 120, 35–50, 2011.
14. Serrano, A. L. C., F. S. Correra, T.-P. Vuong, and P. Ferrari, "Synthesis methodology applied to a tunable patch filter with independent frequency and bandwidth control," *IEEE Transactions on Microwave Theory and Techniques*, Vol. 60, No. 3, 484–493, 2007.
15. Liu, B., F. Wei, and Q.-Y. Wu, "A tunable bandpass filter with constant absolute bandwidth," *Journal of Electromagnetic Waves and Applications*, Vol. 25, Nos. 11–12, 1596–1604, 2011.
16. Huang, X.-G., L. Zhu, Q.-Y. Feng, Q.-Y. Xiang, and D.-H. Jia, "Tunable bandpass filter with independently controllable dual passbands," *IEEE Transactions on Microwave Theory and Techniques*, Vol. 61, No. 9, 3,200–3,208, 2013.
17. Chaudhary, G., Y. Jeong, and Lim, "Harmonic suppressed dual-band bandpass filters with tunable passbands," *IEEE Transactions on Microwave Theory and Techniques*, Vol. 60, No. 7, 2,115–2,123, 2012.
18. Liang, F., X.-F. Zhai, W.-Z. Lu, Q.-X. Wan, and Y.-Y. Zhang, "An independently tunable dual-band filter using asymmetric $\lambda/4$ resonator pairs with shared via-hole ground," *Progress In Electromagnetics Research*, Vol. 146, 99–108, 2014.